JOURNAL OF GEOPHYSICAL RESEARCH, VOL. 105, NO. D4, PAGES 4767–4776, FEBRUARY 27, 2000

Structure and spectral features of the stratospheric aerosol extinction profiles in the UV-visible range derived from SAGE II data

Christine Bingen and Didier Fussen

Belgian Institute for Space Aeronomy, Brussels, Belgium

Abstract. We discuss a climatological model named Extinction Coefficient for Stratospheric Aerosols (ECSTRA), describing the vertical and spectral dependence of the stratospheric aerosol extinction in the UV-visible range. The basic variables used for the analytical formulation of the model are the wavelength, a reduced altitude referenced from the tropopause level, the latitude, and a parameter that describes the volcanic status of the atmosphere. The evolution of the spectral and vertical features of the extinction profile is discussed with respect to the different basic variables. The behavior of the spectral coefficients is qualitatively interpreted as a function of volcanism. The volcanism dependence of the parameters characterizing the Junge layer is also investigated: the peak position shows variations of several kilometers, with a minimum value reached between 0 and 2 km above the tropopause, while the peak width presents a weak volcanism dependence. The most important discrepancies between the model and the SAGE II input data set are found to be related to dynamical effects, and particularly to the influence of the quasi-biennial oscillation.

1. Introduction

Stratospheric aerosols play an important role in the physics and chemistry of the atmosphere. They have an evident influence on the Earth's radiative budget and on the heterogeneous chemistry related to the global ozone depletion [*Russell et al.*, 1996]. It has been shown that aerosols have an influence on the general stratospheric circulation after large eruptions [*Tie et al.*, 1994b; *Kinne et al.*, 1992]. Nevertheless, they remain, in the stratosphere, one of the most difficult compounds to study, due to the great variety of particle sizes, their undefined shape and uncertain composition. The knowledge of those parameters is still important: they can influence significantly the results of simulations including microphysical, chemical, and dynamical effects [*Brasseur et al.*, 1990; *Pitari et al.*, 1993; *Tie et al.*, 1994a; *Weisenstein et al.*, 1997] and hence the selection of realistic scenarios for modeling purposes.

While anthropogenic sources of aerosols have been suggested [*Pitari et al.*, 1993], it is generally accepted that the most important source of stratospheric aerosol is volcanic activity. During major eruptions, a large amount of SO_2 and other species (H_2O, H_2SO_4, H_2S, OCS, HCl, sulphate aerosols, ...) [*Turco et al.*, 1983; *Tie et al.*, 1994a] are injected into the stratosphere up to altitudes of 30 km. SO_2 is oxidized into H_2SO_4 during a reaction sequence producing successively HSO_3 and SO_3. The cycling between SO_2 and H_2SO_4 and the chemistry of sulphur species is described elsewhere [*Weisenstein et al.*, 1997]. During the months just after the eruption, aerosol is produced from H_2SO_4 and water vapor by homogeneous nucleation, condensation, and coagulation processes. The size and composition of the aerosol particles depend on water vapor pressure and temperature [*Steele and Hamill*, 1981], and the composition of volcanic aerosol is estimated to be about 75% H_2SO_4 and 25% H_2O. Sedimentation of the resident particles [*Russell et al.*, 1996; *Weisenstein et al.*, 1997] leads to a progressive decay of the mass loading. Far from large eruptions, aerosol density appears to decrease more slowly toward a possible asymptotic "background aerosol." In fact, large eruptions have been shown to still influence the stratospheric mass loading after many years and even small eruptions can maintain a continuous supply of volcanic aerosol [*Thomason et al.*, 1997b]. Therefore the background level, if any, is probably rarely reached between two major eruptions [*Stothers*, 1996].

Corresponding to this evolution, the mean optical thickness increases rapidly, and after a transient period, decreases to the next major eruption. The decay follows roughly an exponential law with typical relaxation times of about 8 to 25 months.

After the eruption of Mount Pinatubo in June 1991, in situ measurements and remote sounding experiments

Paper number 1999JD901109.
0148-0227/00/1999JD901109$09.00

were realized by means of aircraft, balloon, and satellite [*Pueschel et al.*, 1994; *Brogniez et al.*, 1996; *Thomason et al.*, 1997a]. Those studies give a much better insight of the aerosol properties and microphysical evolution [*Russell et al.*, 1996; *Thomason*, 1992].

Amongst other experiments devoted to aerosol measurements, the Stratospheric Aerosol and Gas Experiment II (SAGE II) was launched in October 1984 and is still operational. This long temporal coverage allowed to cover relaxation periods following several eruptions of rather small, medium, or large importance: Kelut (8° S, 112° E) in February 1990; Ruiz(5° N, 75° W) in November 1985; El Chichón (17° N, 93° W) in November 1992; Pinatubo (15° N, 120° E) in June 1991). Also periods of low activity (around 1989-1990) are included. Therefore SAGE II provides a precious source of measurements over a wide range of volcanic situations, which gave rise to an abundant literature [*McCormick et al.*, 1996; *Thomason et al.*, 1997a]: *Brogniez et al.* [1988] investigated the characteristics of the particle distribution. *Hitchman et al.* [1994] and *Trepte and Hitchman* [1992] studied the aerosol transport by means of the extinction profiles at 1.020 μm. They observed the presence of a tropical reservoir allowing the injection of aerosol into the stratosphere, and a poleward transport mechanism, with aerosol transport along the isentropic surfaces. Other dynamical effects like the rule of quasi-biennial oscillations (QBO) were considered.

Most of those studies do not consider simultaneously the spectral dependence and the vertical structures of the aerosol extinction profile, although *Thomason et al.* [1997a] proposed a global climatology of stratospheric aerosol surface density for 1984-1994 based on a principal component analysis, requiring the four SAGE II spectral channels.

Our contribution to the study of aerosol characteristics consists of the development of a simple and easy-to-handle reference model describing both spectral and vertical features of the aerosol radiative properties in the UV-visible range. Due to its impact on the extinction profile, volcanism is chosen as one of the basic variables of the model. In this way, an analytical model named Extinction Coefficient for Stratospheric Aerosols (ECSTRA) has been developed [*Fussen et al.*, 1998; *Fussen and Bingen*, 1999]. We modeled the aerosol extinction profile as a function of altitude, latitude, wavelength, and a parameter describing the volcanic status of the atmosphere.

In the present work we propose a more detailed description of ECSTRA: we discuss the main spectral and vertical features of the aerosol extinction profile as a function of the basic parameters. We also compare the model results with the SAGE II data and derive an estimation of the ECSTRA error range. After recalling in section 2 the basic ideas of the model, we describe the data processing in section 3. Sections 4 and 5 concern the spectral and vertical dependence of the model, respectively. Finally, section 6 presents the conclusions and outlook for further developments.

2. Theoretical Background

The interaction between light and a spherical particle with an index of refraction m and a radius r comparable to the wavelength λ is described by the Mie theory [*van de Hulst*, 1957]. This general scattering theory allows to determine the extinction cross section $Q(r, \lambda)$ of the particle.

In the case of stratospheric aerosols, the particle size is not constant and a proper size distribution $f(r)$ has to be considered [*Yue*, 1986]. The analytical shape of the distribution and its characteristics (mode radius ρ_m, dispersion σ, and the altitude dependent number density $n(z)$) depends on the volcanism. One of the most used distributions is the lognormal

$$f(r) = \frac{1}{\sqrt{2\pi}r \ln\sigma} \exp\left(-\frac{\ln^2(r/\rho_m)}{2\ln^2\sigma}\right). \quad (1)$$

However, in situ measurements showed that in the case of high volcanism a bimodal or even trimodal [*Pueschel et al.*, 1994] distribution can be observed. The authors cited in this paper (see Table 1) use those particular size distributions, amongst others. At altitude z the related extinction coefficient is given by

$$\beta(z;\lambda) = \int_0^{+\infty} n(z)\ f(r)\ Q(r;\lambda)\ dr. \quad (2)$$

Table 1. Reported Particle Distribution Characteristics in the Post-Pinatubo Period

Month	z, km	Distribution	ρ_m, μm	σ	n, cm^{-3}	Source
August 1991-March 1992	16-20	trimodal	0.10	1.4	1.9	[*Pueschel et al.*, 1994]
			0.33	1.5	2.1	
			0.60	1.3	3.1	
June 1992	20	unimodal	0.38	1.36	...	[*Brogniez et al.*, 1996]
December 1992	21	bimodal	0.25	1.38	5.25	[*Deshler et al.*, 1993]
			0.53	1.17	0.56	
May 1993	20	unimodal	0.27	1.36	...	[*Brogniez et al.*, 1996]

The aerosol optical thickness $\delta(\lambda)$ can be calculated from the extinction coefficient by

$$\delta(\lambda) = \int_{z_t+2\text{ km}}^{+\infty} \beta(z,\lambda)dz. \quad (3)$$

As is usually done, the integration is computed from 2 km above the tropopause level z_t in order to avoid possible contamination by clouds.

Considering that the spectral behavior of β is a slow varying function of the altitude, we used a formal separation of the vertical and spectral dependence:

$$\beta(z;\lambda) = \beta_a(\lambda)\ \beta_b(z). \quad (4)$$

The vertical part $\beta_b(z)$ is defined as the aerosol extinction profile at 1.020 μm. As a consequence, $\beta_a(\lambda = 1.020\ \mu\text{m}) = 1$.

Examining the extinction profile along a meridian reveals a bell-shaped structure centered on the equator [*Hitchman et al.*, 1994]. Therefore it is convenient [*Brogniez and Lenoble*, 1987] to use a reduced altitude z_r with respect to the tropopause:

$$z_r = z - (z_t + 2\text{ km}). \quad (5)$$

Taking into account the roughly linear decreasing of $\ln(\delta(1.020\ \mu\text{m}))$ during the posteruptive relaxation, we defined a volcanism parameter V as representative of the stratospheric aerosol loading:

$$V = \ln(1 + \frac{\bar{\delta}}{\delta_0}) \qquad \delta_0 = 10^{-4}, \quad (6)$$

where $\bar{\delta}$ is the value of $\delta(1.020\ \mu\text{m})$ averaged over the globe and computed by using a 2-month averaging window. The use of a mean value for the optical thickness implies that we do not consider local transient effects.

On the other hand, the averaging describes seasonal effects only through their influence on the basic parameters (particularly, through the tropopause level in (5)). Also, specific microphysical effects observed immediately after a volcanic eruption [*Russell et al.*, 1996; *Thomason*, 1992] and associated to the progressive SO_2 conversion into aerosol droplets are not expected to be correctly described. The volcanism parameter V is intended to be a robust indicator of the global aerosol loading and its mean time evolution. The time evolution of V and related $\bar{\delta}$ are given in Figure 1.

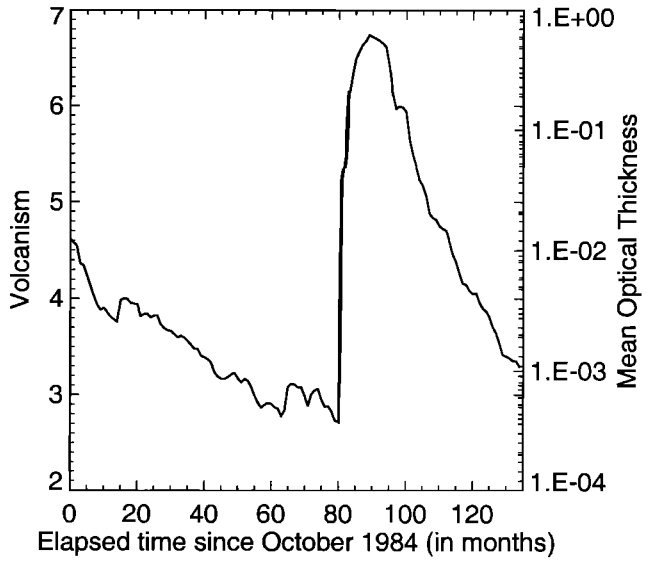

Figure 1. Values of V and $\bar{\delta}$ derived from SAGE II extinctions profiles for the period October 1984 up to December 1995. Read 1.E+00 as 1.0×10^0.

3. Basic Data Set

We used as input data the SAGE II extinction profiles [*Chu et al.*, 1989] from October 1984 up to December 1995. In order to develop the model from a reduced and significant data set, we used a standard binning procedure [*Hitchman et al.*, 1994] that produced a set of reference mean extinction profiles per interval of 1 month in time and 10 degrees in latitude. As far as SAGE II values are available, each bin provides four extinction profiles at the nominal channels λ = 1.020, 0.525, 0.453 and 0.385 μm, and for the standard SAGE II altitude grid (from z=0.5 to 49.5 km with a resolution of 1 km). Within the jth bin the error on the related extinction profile $\beta^{(j)}(z;\lambda)$ is estimated as

$$e_\beta^{(j)}(z;\lambda) = \sqrt{\sigma_S^{(j)}(z;\lambda)^2 + \sigma_P^{(j)}(z;\lambda)^2}, \quad (7)$$

where $\sigma_S^{(j)}(z;\lambda)$ is the standard deviation related to SAGE II extinction errors, and $\sigma_P^{(j)}(z;\lambda)$ is the standard deviation of the event population at altitude z and wavelength λ in bin j.

For the kth SAGE II event integrating $\beta^{(k)}(z;\lambda)$ by using (3) provides a value $\delta^{(k)}(\lambda)$ of the optical thickness, and the corresponding tropopause $z_t^{(k)}$ is derived from the measured temperature profile. These values are averaged in a similar way so that a set of mean values of $\delta^{(j)}(\lambda)$ and $z_t^{(j)}$ can be associated with the jth bin. If no extinction profile is available at low altitude for a given bin (due to instrument saturation, for instance), another method must be applied in order to estimate the corresponding $\delta^{(j)}(\lambda)$ and $z_t^{(j)}$. Therefore we extrapolated the primitive

$$\tilde{\delta}^{(j)}(z;\lambda) = \int_z^{+\infty} \beta^{(j)}(z';\lambda)dz', \quad (8)$$

by means of the error function erf(z). This extrapolation can only succeed if the available extinction profile reaches its maximal value at the level of the Junge layer. Otherwise, no estimation of $\delta^{(j)}(\lambda)$ is retained. When

$z_t^{(j)}$ is lacking, we used a mean value of the tropopause level representative for the considered bin.

4. Spectral Dependence

4.1. Formulation

The spectral dependence of the extinction coefficient has been modeled by

$$\beta_a(\lambda) = \exp\left(a_1 \Delta\lambda + a_2 \Delta\lambda^2\right), \qquad (9)$$

where $\Delta\lambda = \lambda - 1.020$ μm. This formulation proposed by *Yue* [1986] is a positive function of minimal complexity able to describe the change of spectral behavior corresponding to all possible volcanic ranges. In particular, a typical "background" aerosol situation is characterized by a monotonic and possibly steep decrease of β_a versus λ. On the contrary, a highly volcanic stratosphere may exhibit extinction profiles with a clear extremum in the UV-visible range.

For the jth bin a set of $\left\{a_1^{(j)}, a_2^{(j)}\right\}$ was determined by means of a weighted linear least squares fitting algorithm applied to $\ln(\beta_a(\lambda))$. The error $e_\beta^{(j)}$ given by (7) is used for the computation of the weights, according to standard procedures of the error theory.

The dependence of a_1, a_2 on V, z_r and latitude φ is modeled by

$$a_i = \sum_{j=0}^{2} \sum_{k=0}^{2} \sum_{l=0}^{3} \alpha_{ijkl}\, P_{2j}(\theta)\, V^k\, {z_r}^l, \qquad (10)$$

where $\theta = \frac{\pi}{2} - \varphi$ is the colatitude and $\{P_0, P_2, P_4\}$ are symmetric Legendre polynomials. The solution of (10) was computed from all available $\left\{a_1^{(j)}, a_2^{(j)}\right\}$ by a singular value decomposition algorithm. The values of the spectral fit coefficients have been published elsewhere [*Fussen and Bingen*, 1999].

4.2. Discussion

Typical spectral dependences of β_a are given in Figure 2 for different values of the volcanism. It can be noticed that, as already mentioned, β_a is a decreasing function of λ at low volcanism. Corresponding to this, a_1 is negative and a_2 becomes close to zero when V is decreasing. From the Mie scattering theory, it can be seen that this case is encountered when particles are small compared to the wavelength. For the year 1979 characterized by a low volcanic level, *Brogniez and Lenoble* [1987] found typical particle mode radii of about 0.10 to 0.17 μm depending on the season. *Yue and Deepak* [1984] reported ρ_m values of 0.05 to 0.10 μm for the same period. In both cases, ρ_m is effectively small compared to λ.

At high volcanism, the density of particles increases by a factor 10 or more. A good overview of the evolution of the particle size distribution after the Pinatubo eruption is proposed by *Russell et al.* [1996, and references therein]. They observe, immediately after the eruption, the greatest relative increase in particle density for the smallest ($r < 0.2$ μm) and the largest ($r > 0.6$ μm) particles, corresponding to fresh aerosol nuclei and to ash particles, respectively. Just above the tropopause the authors mention a third mode corresponding to coated ash particles. Thomason also found the simultaneous presence of three modes at midlatitude in the low stratosphere, approximately from July 1991 to October 1991 [*Thomason*, 1992]. *Pueschel et al.* [1994] observed a trimodal distribution between 9.5 and 20.2 km during the period January to March 1992. *Deshler et al.* [1993] observed bimodal particle distributions up to January 1993, with a progressive increase of the mode radii and dispersion associated with a decrease of the particle density. *Brogniez et al.* [1996] used a lognormal distribution and found quite large values of ρ_m in May 1993. Some reported distributions parameters are given in Table 1. Through all those observations, large particles are found to be present during at least 2 years following the Pinatubo eruption. Just above the tropopause, mode radii seem to grow during up to 2 years due to coagulation mechanism, even if the particle density decreases due to gravitational sedimentation.

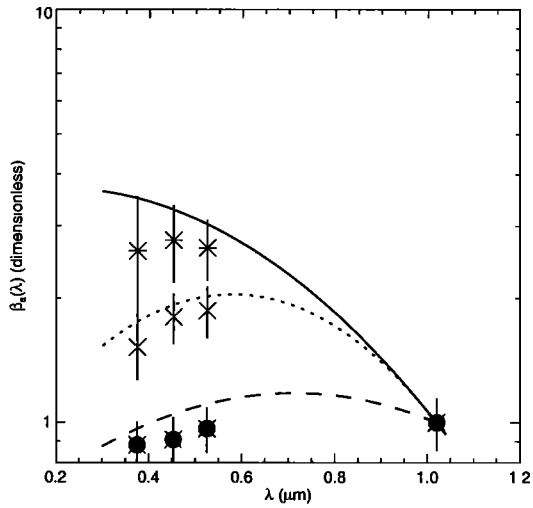

Figure 2. Spectral dependence of β_a at $z_r = 5$ *km* for SAGE II observations (symbols) and related spectral curve computed by ECSTRA (lines), on April 2, 1989 (asterisk, solid; $\varphi = 8.0°$S; $V = 3.1$), September 9, 1993 (cross, dotted; $\varphi = 0.2°$S; $V = 4.88$), and July 4, 1992 (solid circle, dashed; $\varphi = 4.4°$S; $V = 6.65$).

Corresponding to this evolution, very flat spectral dependences are observed at high volcanism values, related to values of a_1, a_2 close to zero. When the volcanism decreases, the mean slope of the spectral dependence increases, giving rise at first to a more pronounced curvature a_2 of $\ln(\beta_a)$. At low values of V the spectral dependence tends to the "background" characteristics described above.

This typical behavior was previously described by *Brogniez et al.* [1996] and can be understood from the

Mie scattering theory. It is well described by ECSTRA, as it can be seen in Figure 3.

The dependence of a_1 and a_2 on time and latitude simulated by ECSTRA is given in Figures 4 and 5 for $z_r = 5$ km. Again, the same qualitative behavior as described above is observed after the main volcanic eruptions (El Chichón, 11 months before October 1984; Pinatubo, 81 months after October 1984). The corresponding values of $\left\{a_1^{(j)}, a_2^{(j)}\right\}$, not represented here, approach rapidly zero during the 5 months following the eruption. In November and December 1991 (86 and 87 months after October 1984), positive values of $\left\{a_1^{(j)}, a_2^{(j)}\right\}$ are observed in the neighborhood of the eruption. *Lenoble and Brogniez* [1985] found such a curvature inversion to be possibly related with the presence of a bimodal size distribution. Afterwards, both $\left\{a_1^{(j)}, a_2^{(j)}\right\}$ decrease again. Variable $a_1^{(j)}$ is found to approach -3 or -3.5 after 13 to 15 months at all latitudes, whereas $a_2^{(j)}$ presents variations at midlatitudes related with seasonal effects. The same dependences described by ECSTRA in Figures 4 and 5 show similar general features. As expected, the model is, however, not able to reproduce correctly the transient effects immediately after the eruption. Therefore the rapid growth of $a_2^{(j)}$ during the first months after June 1991, and the positive values of $\left\{a_1^{(j)}, a_2^{(j)}\right\}$ and the end of 1991, are not reproduced by ECSTRA. Also the seasonal effects affecting more particularly $a_2^{(j)}$ at midlatitudes are smoothed out.

Although no dynamic effect is taken into account by ECSTRA, the effects of transport on the latitudinal aerosol distribution are fairly well observed. As previously pointed out by *Trepte et al.* [1994] and *Tie et al.* [1994b], the important upwards motions in the tropics can favor a rapid transport of aerosol. Due to the Brewer-Dobson circulation, the aerosol particles migrate to higher latitudes. In those regions, vertical motion is very limited, so that gravitational sedimentation,

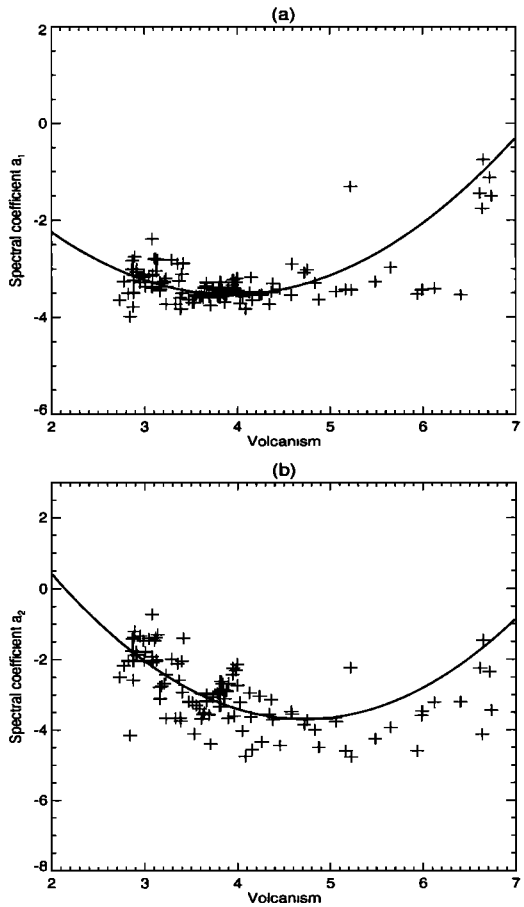

Figure 3. Dependence on the volcanism V of the spectral fit coefficients (a) a_1 and (b) a_2 at $\varphi = 5°$S and $z_r = 5$ km. The solid line and symbols represent the ECSTRA result and the related $a_i^{(j)}$ values, respectively.

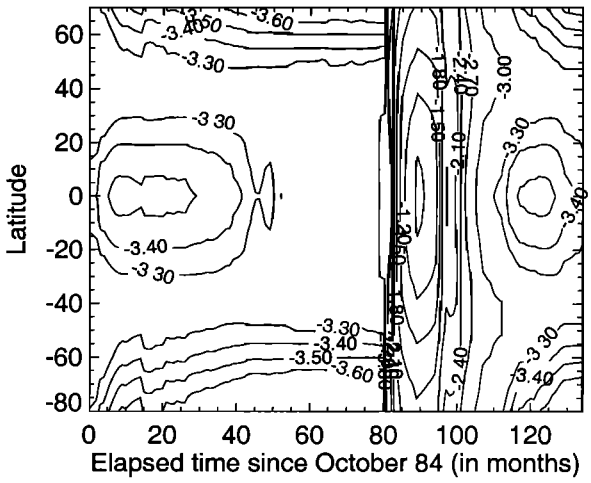

Figure 4. Dependence of a_1 on time and latitude at $z_r = 5$ km, simulated by ECSTRA.

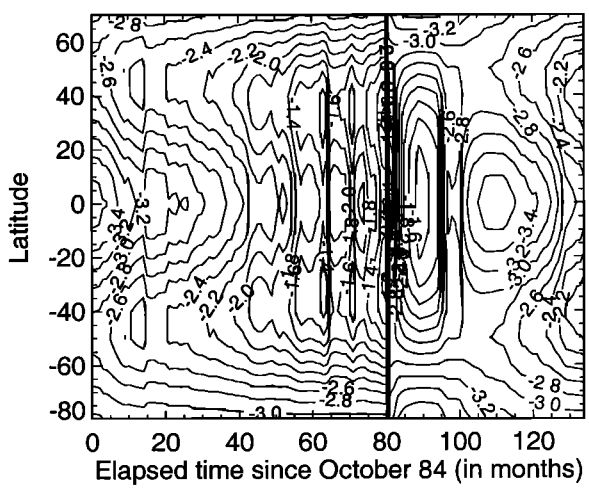

Figure 5. Dependence of a_2 on time and latitude at $z_r = 5$ km, simulated by ECSTRA.

characterized by a long time constant (> 1 year [*Kasten*, 1968]), becomes the major source of aerosol decay. Corresponding to this, the a_i coefficients are found to decay much more slowly at high latitude than at low latitude. The presence of the tropical reservoir described by *Hitchman et al.* [1994] and *Trepte et al.* [1992, 1994] is also well represented by ECSTRA.

A comparison has been made between the SAGE II binned input data and the ECSTRA results, by defining the relative error as

$$\varepsilon_i = \left| \frac{(a_i^{\mathrm{SAGE}}) - (a_i^{\mathrm{ECSTRA}})}{(a_i^{\mathrm{SAGE}})} \right|. \qquad (11)$$

Principal features are shown in Figure 6. The spectral fitting can be considered as valid in the range $\delta = [1.5 \times 10^{-3}, 10^{-1}]$, $\varphi = [80°\mathrm{S}, 80°\mathrm{N}]$ and $z_r = [0, 20\ \mathrm{km}]$. Within this range a global mean error $\bar{\varepsilon}_i$ has been estimated for both error parameter ε_i after removing outliers. For reduced altitudes, z_r = 0, 5, 10, and 15 km, $\bar{\varepsilon}_1$ was found to be about 2.1, 0.2, 0.2, and 0.3, respectively, and $\bar{\varepsilon}_2$ was found to be about 1.7, 0.4, 1.2, and 1.4.

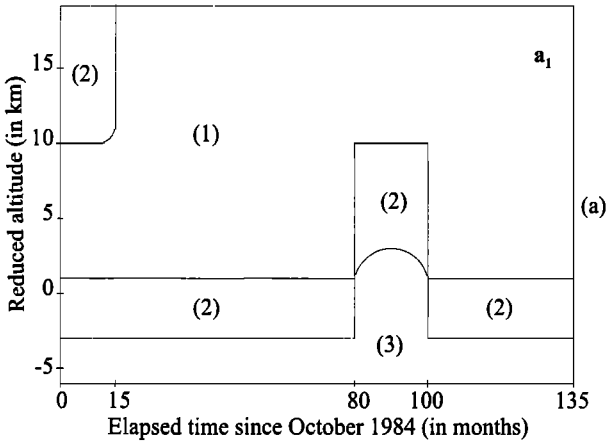

(1) $\varepsilon_1 \leq 0.2$ (with possibly limited regions with $\varepsilon_1 \sim 0.5$ at $z_r > 10$ km)
(2) $\varepsilon_1 \geq 2.5$ at low latitudes; $\varepsilon_1 \leq 0.2$ elsewhere; instabilities observed around the tropopause level
(3) Fit not valid or impossible

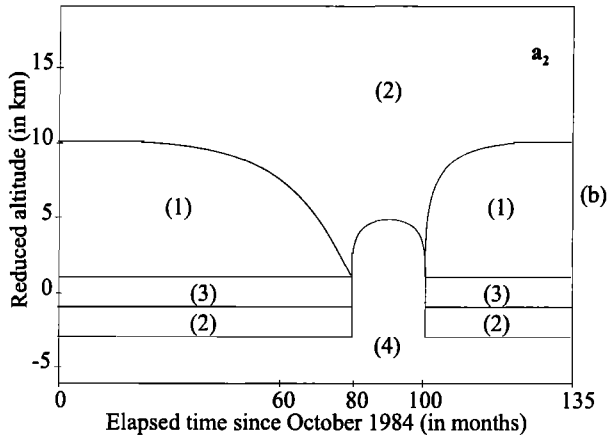

(1) $\varepsilon_2 \leq 0.4$ to 0.6
(2) $\varepsilon_2 \leq 1$ to 2; instabilities with $\varepsilon_2 \geq 4$
(3) $\varepsilon_2 \leq 4$; many instabilities with greater ε_2 values
(4) Fit not valid or impossible

Figure 6. Dependence on φ and z of (a) ε_1 and (b) ε_2.

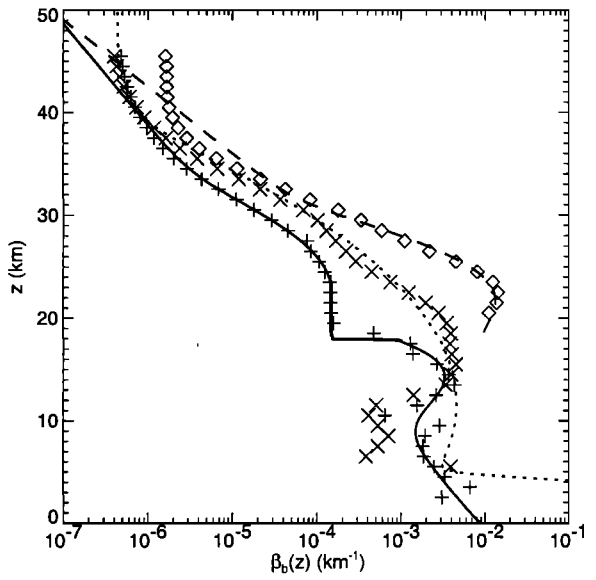

Figure 7. Vertical extinction profile β_b for April 1989 (pluses, solid; V = 3.1), September 1993 (crosses, dotted; V = 4.88), and July 1992 (diamonds, dashed; V = 6.65); φ = 15°N. Symbols and lines represent the SAGE II binned profile and the corresponding fit by means of a Levenberg-Marquardt algorithm, respectively.

5. Vertical Dependence

5.1. Formulation

In the troposphere the vertical extinction coefficient is dominated by pronounced and variable structures related to the cloud contribution. Above this region the structure becomes much more stable. After an eventual steep transition at the tropopause level, the extinction profile shows a peak referred to as the Junge layer, situated a few kilometers above z_t. At higher altitudes ($z \gtrsim 30$ km) the profile exhibits a slope change and approaches asymptotically an exponential decrease (see Figure 7).

In order to clearly describe those structures, the vertical extinction coefficient β_b has been modeled by

$$\begin{aligned} \beta_b(z_r) &= \beta_{\mathrm{aero}}(z_r) + \beta_{\mathrm{cloud}}(z_r) \quad z_r < 0 \\ \beta_b(z_r) &= \beta_{\mathrm{aero}}(z_r) \quad z_r \geq 0, \end{aligned} \qquad (12)$$

where

$$\beta_{\mathrm{aero}}(z_r) = e^{x_1 + x_2\, z_r} + e^{x_3 - [(z_r - x_4)/x_5]^2}, \qquad (13)$$

$$\beta_{\mathrm{cloud}}(z_r) = e^{x_6 + x_7\, z_r + x_8\, {z_r}^2 + x_9\, {z_r}^3}. \qquad (14)$$

The first term of the aerosol contribution β_{aero} stands for the high-altitude asymptotic behavior. The second term represents a Gaussian peak of amplitude exp (x_3) and width x_5, centered at altitude x_4 and associated with the Junge layer. The cloud contribution β_{cloud} has been taken into account in order to allow the free determination of the aerosol parameters $\{x_i, i = 1, \cdots, 5\}$. All the fit coefficients $x_1, \cdots, x_9$ were found to be functions of the latitude, whereas x_1, x_2; x_6, x_7, x_8, x_9 are independent on the volcanism. Again, the formulation of β_b has the advantage to be naturally positive constrained. Typical examples of vertical profiles are illustrated in Figure 7.

Integrating (3) by using (12), (13), and (14) gives

$$\delta(1.020\ \mu\text{m}) = -\frac{e^{x_1}}{x_2} + e^{x_3}\frac{\sqrt{\pi}}{2}x_5\left[1 + \text{erf}\left(\frac{x_4}{x_5}\right)\right]. \quad (15)$$

The first term of (15) does not depend on the volcanism level. By analogy to (6) we defined some minimal volcanism level $V_{\min}$ from this term as

$$V_{\min} = \ln\left(1 - \frac{e^{x_1}}{\delta_0 x_2}\right). \quad (16)$$

The computation of $x_1, \cdots, x_9$ from the SAGE II binned profiles is a nonlinear least squares problem for which we used a Levenberg-Marquardt algorithm. For each bin j successfully processed (97% of the valid profiles), a set of optimal $\left\{x_1^{(j)}, \cdots, x_9^{(j)}\right\}$ was determined.

Further, it is useful to introduce the following algebraic transformation for the formulation of the general fit problem of $\{x_1, \cdots, x_9\}$ by means of all the available $\left\{x_1^{(j)}, \cdots, x_9^{(j)}\right\}$:

$$V_{\min} = u_1, \quad (17)$$

$$-\frac{1}{x_2} = u_2, \quad (18)$$

$$\frac{x_4}{x_5} = u_{45} + v_{45}\Delta V^2 + w_{45}\Delta V^3, \quad (19)$$

$$\frac{1}{x_5} = u_5 + v_5\Delta V^2, \quad (20)$$

$$x_6 = u_6, \quad (21)$$

$$x_7 = u_7, \quad (22)$$

$$x_8 = u_8, \quad (23)$$

$$x_9 = u_9, \quad (24)$$

$$\Delta V = (V - V_{\min}). \quad (25)$$

All the fit coefficients u_i, v_i, w_i have been given a latitudinal dependence through an expansion in terms of the symmetric Legendre polynomials $\{P_0(\theta), P_2(\theta), P_4(\theta)\}$.

The left-hand sides of (17)-(24) were chosen for their rather smooth variation that can be reasonably described by simple analytic functions over the whole considered volcanic range. The fit coefficient values u_i, v_i, w_i have been published previously [*Fussen and Bingen*, 1999].

5.2. Discussion

In order to check the physical significance of the peak parameters $\{x_3, x_4, x_5\}$, an alternative way has been carried out for the computation of the peak amplitude, position, and width of the Junge layer: Each SAGE II binned profile has been smoothed out by means of a constrained cubic spline β_b^S of minimal curvature. We determined the amplitude $exp\,(x_3^S)$ and position x_4^S of the spline maximum, and we derived an estimation of the spline peak width x_5^S by an adequate least squares fit procedure. We found spline parameters x_3^S, x_4^S, and x_5^S in fairly good agreement with the corresponding peak parameters x_3, x_4, and x_5.

The behavior of x_3, x_4, x_5 can be visualized in Figure 8. The description of the volcanism dependence of x_3 is very satisfactory, and the asymptotic behavior of x_3 should be correctly described for extreme values of the volcanism. On the contrary, the choice of the fit functions cannot guarantee an accurate description of x_4 and to $1/x_5$ beyond the volcanism range of the available data.

The dependence of x_4 on the volcanism shows that, whereas the aerosol layer is situated a few kilometers above the tropopause level at low volcanism, the peak position decreases when V increases, and reaches a minimum value around reduced altitudes of 0 to -2 km at $V \simeq 5$. For higher volcanism values, the peak position grows again and moves away far from the tropopause level. This volcanism dependence of the peak position, and particularly the presence of a minimum value around $V = 5$ is observed through the behavior of the x_4, $x_4^{(j)}$, and x_4^S as well. The minimum value of x_4 has been found to be about -0.4 to -0.7 km at low and middle latitude and to decrease up to -1.4 to -1.8 km near the polar regions. An examination of the latitudinal dependence of $x_4^{(j)}$ reveals similar characteristics. However, the minimum value of $x_4^{(j)}$ presents a steep increase around 40°S and 40°N, which is not described by the general fit parameter x_4 due to the limited Legendre polynomials expansion.

The presence of a minimum in the volcanism dependence of the peak position is probably due to mechanisms of gravitational sedimentation (see above) taking place after volcanic eruptions [*Deshler et al.*, 1992, 1993; *Tie et al.*, 1994a], and which could induce a slow descent of the Junge layer [*Tie et al.*, 1994b]. The major role played by sedimentation at high latitude and the absence of important vertical air motions in the same regions could explain the extreme values of the minimum near the poles. On the contrary, the regions below 60° in both hemispheres are characterized by a significant meridional transport at midlatitude and by strong vertical motions within the tropical reservoir. In those regions the role of sedimentation is less important, and the minimum value of x_4 is expected to be higher.

The width of the Junge layer x_5 is found to exhibit a slow decrease as volcanism increases; x_5 seems to ap-

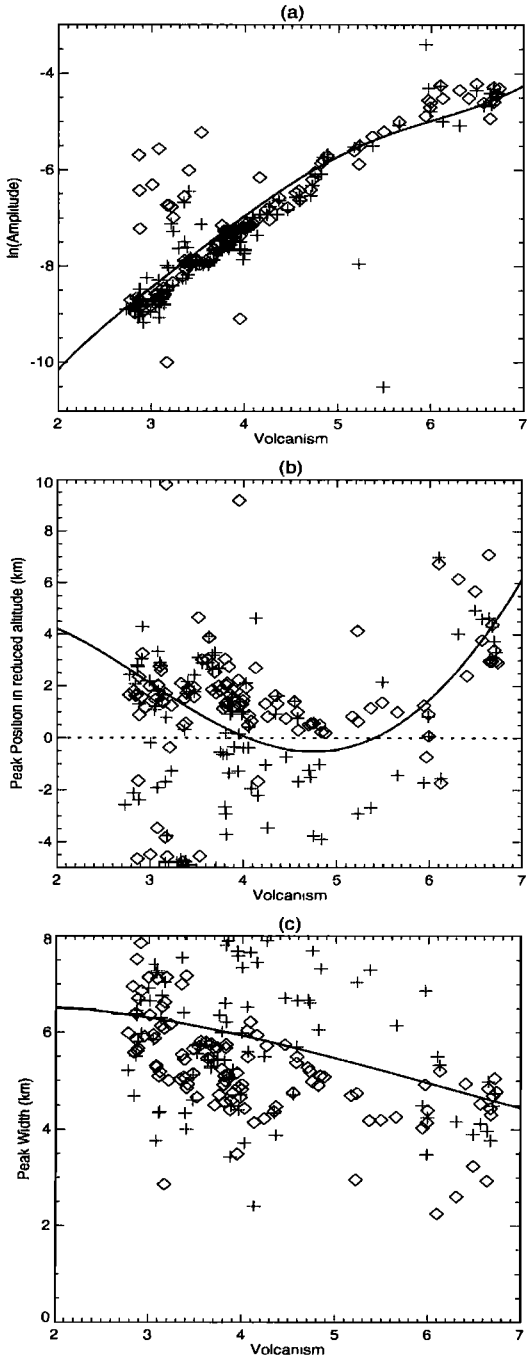

Figure 8. Comparison of the peak parameters retrieved from the Levenberg-Marquardt fit (pluses), from the cubic spline smoothing (diamonds), and the general fit of x_i (solid line): (a) amplitude ($\exp(x_3)$, $\exp(x_3^S)$), (b) position (x_4, x_4^S), and (c) width (x_5, x_5^S). The parameters are plotted as a function of volcanism for $\varphi = 20°$N.

proach a constant value for low values of V. If the behavior of x_3, x_4, and x_5 shows an evident dependence on the volcanism, the $x_4^{(j)}$ and $x_5^{(j)}$ values show a relatively high dispersion around the ECSTRA simulation curve. The reason of this dispersion can be derived by examining Figure 9.

During the whole load decay period preceding the Pinatubo eruption, the temporal evolution of $x_4^{(j)}$ shows successive extrema which are not reproduced by ECSTRA. Those peaks are due to the influence of the QBO on the aerosol transport in the stratosphere. Transport effects on the aerosol distribution were studied by

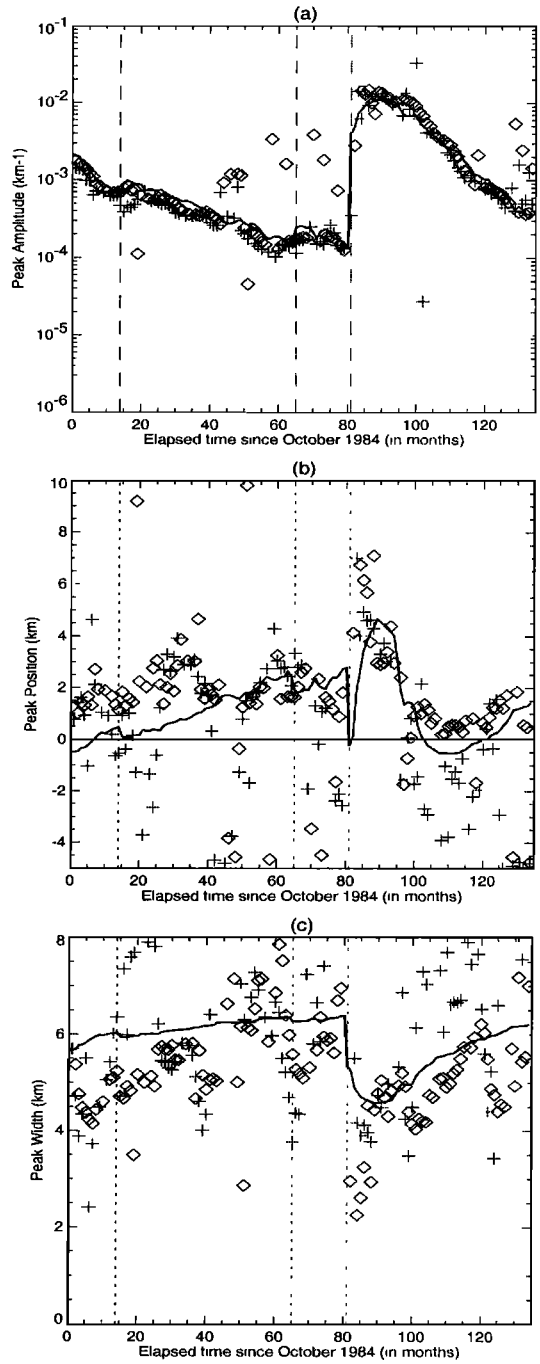

Figure 9. Time dependence of the peak parameters retrieved from the Levenberg-Marquardt fit (pluses), from the cubic spline smoothing (diamonds), and from ECSTRA (solid line): (a) amplitude ($\exp(x_3)$, $\exp(x_3^S)$), (b) position (x_4, x_4^S), and (c) width (x_5, x_5^S). The parameters are plotted for $\varphi = 20°$N. The dashed lines indicate the eruption time of Ruiz, Kelut, and Pinatubo.

Hitchman et al. [1994]. They show that during the easterly shear the QBO induces an equatorial lofting due to the presence of westward winds increasing with the altitude, and a confinement of the aerosol between the tropics in the lower stratosphere. On the other side, the QBO westerly shear is characterized by an equatorial subsidence and a meridional poleward spreading of the aerosol mass in the lower stratosphere. From the determination of the dominant sign of the vertical shear at the equator, the authors identified the periods associated with the two phases of the QBO, up to end 1990. They found the periods associated to the easterly shear to be the periods October 1985 to April 1987 (months 13 to 31 referred to as October 1984, see Figure 9) and March 1988 to July 1989 (months 42 to 58). Periods associated with the westerly shear are October 1984 to September 1985 (months 1 to 12), May 1987 to February 1988 (months 32 to 41), and August 1989 to October 1990 (months 59 to 73). It can be seen in Figure 9 that the increasing periods of $x_4^{(j)}$ and $x_5^{(j)}$ are directly related to the ascent characterizing the easterly shear, whereas a decrease of $x_4^{(j)}$ and $x_5^{(j)}$ is observed during the westerly shear. The same observation can be done on the corresponding x_4^S and x_5^S spline parameters. The peak amplitude exp (x_3) seems to be weakly affected by seasonal effects. More particularly, there is no significant influence of the QBO on the peak amplitude.

As given previously, an estimation of the error has been achieved between the SAGE II binned input data and the ECSTRA results. Therefore an error parameter has been defined as

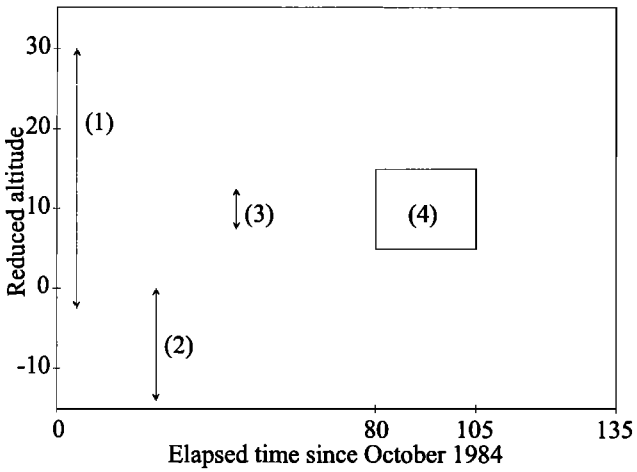

Figure 10. Dependence on time, φ, and z_r of the error parameter E_R. 1, In the tropical region, $E_R \sim 0.05$ to 0.2 at $z_r > 15$ km and $E_R \leq 0.06$ at $z_r < 15$ km; $E_R \leq 0.06$ in the subtropics and $E_R \leq 0.08$ to 0.12 in the extratropical regions. 2, For $\varphi = 30°$S to 30°N, $E_R \leq 0.07$ at $z_r > -10$ km and $E_R \sim 0.5$ to 1 at $z_r < -10$ km; $E_R \sim 0.5$ to 1 in the extratropical regions. At midlatitude, $E_R \leq 0.3$ just below the tropopause. 3, $E_R \sim 0.1$ tot 0.2 in some time periods at $\varphi = 40°$N to 50°N. 4, $E_R \sim 0.3$, or even locally $E_R \sim 0.8$.

$$E_R = \left| \frac{\log(\beta_{\mathrm{SAGE}}) - \log(\beta_{\mathrm{ECSTRA}})}{\log(\beta_{\mathrm{SAGE}})} \right|. \quad (26)$$

A formulation based on the logarithm of the extinction coefficient has been chosen in order to allow an estimation of the discrepancy between both profiles over the whole range of the extinction values ($\simeq 10^{-7}$ to 10^{-1} km^{-1}). An overview of the error estimation is reported in Figure 10. It must be pointed out that the error below the tropopause level refers to a mean cloud coverage for the related month, as described by the SAGE II binned profiles. Due to the great variability of this coverage, an important discrepancy between an isolated event and the mean cloud coverage can be observed. Figure 10 shows that ECSTRA can be considered as valid for the whole stratosphere. Nevertheless, it must be noticed that the error parameter E_R can increase to about 0.8 at midaltitude during a limited period following the Pinatubo eruption. The global mean error $\overline{E_R}$ obtained after removing outliers is about $\overline{E_R} = 0.08$ in the extratropical regions and can reach $\overline{E_R} = 0.11$ at the equator.

6. Conclusions

The ECSTRA model has been previously proposed for describing the vertical and spectral dependences of the aerosol extinction profile as a function of latitude, altitude, wavelength, and volcanism [*Fussen and Bingen*, 1999]. In the present work we have investigated the behavior of the various parameters of ECSTRA as functions of those basic variables. We show that ECSTRA is able, out of transients following volcanic eruptions, to reproduce on a reliable way the vertical structures of the extinction profiles and also the general spectral features associated with the four SAGE II channels. A systematic investigation of the error led to the determination of the model validity range. Concerning the position and width of the Junge layer, we identify some discrepancies between the ECSTRA simulations and the cubic spline description as due to the influence of the QBO.

In spite of its inability to describe correctly those dynamical effects, ECSTRA has been shown to be a useful and robust tool giving insight on general features of the stratospheric extinction profiles for a wide range of volcanic situations. Therefore, although this simple model is only a fitting procedure that cannot reflect the whole complexity of the aerosol physics, we think that ECSTRA can be used for interpretation and simulation purposes of general features concerning stratospheric aerosols.

In this perspective, different aspects require further investigations. Concerning the spectral dependence, ECSTRA gives us a tool for studying the aerosol particle characteristics (mean size and dispersion), as a function of the considered basic parameters. However, the severe limitation of the information content due to the restricted spectral range has to be taken into account.

The vertical features emerging from the model could also be the subject of further studies. Finally, the evolution of the characteristic parameters of the Junge layer described by ECSTRA should be interpreted in terms of the dynamical evolution of the aerosol microphysics.

Acknowledgments. The SAGE II data were obtained from the NASA Langley Research Center - EOSDIS Distributed Active Archive Center. This work was also partly supported by the Fonds National de la Recherche Scientifique under grant 1.5.155.98.

References

Brasseur, G., M. H. Hitchman, S. Walters, M. Dymek, E. Falise, and M. Pirre, An interactive chemical dynamical radiative two-dimensional model of the middle atmosphere, *J. Geophys. Res., 95,* 5639-5655, 1990.

Brogniez, C., and J. Lenoble, Modeling of the stratospheric background aerosols from zonally averaged SAGE profiles, *J. Geophys. Res., 92,* 3051-3060, 1987.

Brogniez C., and J. Lenoble, Size distribution of stratospheric aerosols from SAGE II multiwavelength extinctions, in *Aerosols and Climate*, edited by P.V. Hobbs and M. P. McCormick, pp. 305-311, A. Deepak, Hampton, Va., 1988.

Brogniez, C., J. Lenoble, M. Herman, P. Lecomte, and C. Verwaerde, Analysis of two balloon experiments in coincidence with SAGE II in case of large stratospheric aerosol amount: Post-Pinatubo period, *J. Geophys. Res., 101,* 1541-1552, 1996.

Chu, W. P., M. P. McCormick, J. Lenoble, C. Brogniez, and P. Pruvost, SAGE II inversion algorithm, *J. Geophys. Res., 94,* 8339-8351, 1989.

Deshler, T., D.J. Hofmann, B.J. Johnson, and W.R. Rozier, Balloonborne measurements of the Pinatubo aerosol size distribution and volatility at Laramie, Wyoming, during the summer of 1991, *Geophys. Res. Lett., 19,* 199-202, 1992.

Deshler, T., B.J. Johnson, and W.R. Rozier, Balloonborne measurements of the Pinatubo aerosol during 1991 and 1992 at 41°N: Vertical profiles, size distribution, and volatility *Geophys. Res. Lett., 20,* 1435-1438, 1993.

Fussen D., and C. Bingen, A volcanism dependent model for the extinction profile of stratospheric aerosols in the UV-visible range, *Geophys. Res. Lett., 26,* 703-706, 1999.

Fussen, D., C. Bingen, and F. Van Hellemont, A climatological model for the extinction coefficient of stratospheric aerosols, in *SPIE Proceedings of Earth's Observing Systems III, 19-24 July 1998, San Diego, 3439,* 578-584, 1998.

Hitchman, M. H., M. McKay, and C. R. Trepte, A climatology of stratospheric aerosol, *J. Geophys. Res., 99,* 20,689-20,700, 1994.

Kasten, F., Falling speed of aerosol particles, *J. Appl. Meteorol., 7,* 944-947, 1968.

Kinne, S., O. B. Toon, and M. J. Prather, Buffering of stratospheric circulation by changing amounts of tropical ozone: A Pinatubo case study, *Geophys. Res. Lett., 19,* 1927-1930, 1992.

Lenoble, J., and C. Brogniez, Information on stratospheric aerosol characteristics contained in the SAGE satellite multiwavelength extinction measurements, *Appl. Opt., 24,* 1054-1063, 1985.

McCormick, M. P., P.-H. Wang, and M. C. Pitts, Background stratospheric aerosol and polar stratospheric cloud reference models, *Adv. Space Res., 18,* 155-177, 1996.

Pitari, G., V. Rizi, L. Ricciardulli, and G. Visconti, High-speed civil transport impact: Role of sulfate, nitric acid trihydrate, and ice aerosols studied with a two-dimensional model including aerosol physics, *J. Geophys. Res., 98,* 23,141-23,164, 1993.

Pueschel, R. F., P. B. Russell, D. A. Allen, G. V. Ferry, and K. G. Snetsinger, Physical and optical properties of the Pinatubo volcanic aerosol: Aircraft observations with impactors and a Sun-tracking photometer, *J. Geophys. Res., 99,* 12,915-12,922, 1994.

Russell, P. B., et al., Global to microscale evolution of the Pinatubo volcanic aerosol, derived from diverse measurements and analyses, *J. Geophys. Res., 101,* 18,745-18,763, 1996.

Steele, H. M., and P. Hamill, Effects of temperature and humidity on the growth and optical properties of sulfuric acid-water droplets in the stratosphere, *J. Aerosol Sci., 12,* 517-528, 1981.

Stothers, R. B., Major optical depth perturbations to the stratosphere from volcanic eruptions: Pyrheliometric period, 1881-1960, *J. Geophys. Res., 101,* 3901-3920, 1996.

Thomason, L. W., Observations of a new SAGE II aerosol extinction mode following the eruption of Mt. Pinatubo, *Geophys. Res. Lett., 19,* 2179-2182, 1992.

Thomason, L. W., L. R. Poole, and T. Deshler, A global climatology of stratospheric aerosol surface area density deduced from Stratospheric Aerosol and Gas Experiment II measurements: 1984-1994, *J. Geophys. Res., 102,* 8967-8976, 1997a.

Thomason, L. W., G. S. Kent, C. R. Trepte, and L. R. Poole, A comparison of the stratospheric aerosol background periods of 1979 and 1989-1991, *J. Geophys. Res., 102,* 3611-3616, 1997b.

Tie, X., X. Lin, and G. Brasseur, Two-dimensional coupled dynamical/chemical/microphysical simulation of global distribution of El Chichón volcanic aerosols, *J. Geophys. Res., 99,* 16,779-16,792, 1994a.

Tie, X., G. P. Brasseur, B. Briegleb, and C. Granier, Two-dimensional simulation of Pinatubo aerosol and its effect on stratospheric ozone, *J. Geophys. Res., 99,* 20,545-20,562, 1994b.

Trepte, C. R., and M. H. Hitchman, Tropical stratospheric circulation deduced from satellite aerosol data, *Nature, 355,* 626-628, 1992.

Trepte, C. R., L. W. Thomason, and G. S. Kent, Banded structures in stratospheric aerosol distributions, *Geophys. Res. Lett., 21,* 2397-2400, 1994.

Turco, R. P., O. B. Toon, R. C. Whitten, P. Hamill, and R. G. Keesee, The 1980 eruptions of Mount St. Helens: Physical and chemical processes in the stratospheric clouds, *J. Geophys. Res., 88,* 5299-5319, 1983.

van de Hulst, H. C., *Light Scattering by Small Particles,* Dover, Mineola, N. Y., 1957.

Weisenstein, D. K., G. K. Yue, M. K. W. Ko, N. D. Sze, J. M. Rodriguez, and C. J. Scott, A two-dimensional model of sulfur species and aerosols, *J. Geophys. Res., 102,* 13,019-13,035, 1997.

Yue, G. K., and A. Deepak, Latitudinal and altitudinal variation of size distribution of stratospheric aerosols inferred from SAGE aerosol extinction coefficient measurements at two wavelengths, *Geophys. Res. Lett., 11,* 999-1002, 1984.

Yue, G. K., Wavelength dependence of aerosol extinction coefficient for stratospheric aerosols, *J. Clim. Appl. Meteorol., 25,* 1775-1779, 1986.

C. Bingen and D. Fussen, Belgian Institute for Space Aeronomy (IASB-BIRA), 3, avenue Circulaire, B-1180, Brussels, Belgium. (Christine.Bingen@oma.be; Didier.Fussen@oma.be)

(Received March 9, 1999; revised September 14, 1999; accepted October 26, 1999.)